J Polym Environ (2018) 26:1979–1985
DOI 10.1007/s10924-017-1095-1

ORIGINAL PAPER

Fabrication of Polypyrrole/Chitosan Nanocomposite Aerogel Monolith for Removal of Cr(VI)

Jiayou Ji[1] · Huizhi Xiong[1] · Zhenni Zhu[1] · Liang Li[1] · Yineng Huang[2] · Xianghua Yu[1]

Published online: 14 August 2017

Abstract Three-dimensional polypyrrole/chitosan nanocomposite monoliths are fabricated by polymerization of pyrrole in chitosan aqueous solution. The static polymerization of pyrrole monomer and the cross-linking of chitosan by glutaraldehyde occur simultaneously, resulting in the self-assembly of polypyrrole/chitosan nanocomposite aerogel monolith. The addition of methyl orange and glutaraldehyde and the static reaction play key roles in the formation of the self-standing aerogel monolith. The as-prepared monolith with larger specific surface area exhibits much better adsorption capability for Cr(VI) removal in comparison with that prepared without the addition of glutaraldehyde. The adsorption process and adsorption isotherms are found to well follow the pseudo-second-order and Langmuir models, respectively. Furthermore, this polypyrrole/chitosan nanocomposite monolith is stable and recyclable. About 73.5% of the initial adsorption capability is kept after eight adsorption–desorption cycles. The polypyrrole/chitosan nanocomposite monolith can be a promising candidate for the efficient removal of Cr(VI).

Keywords Polypyrrole · Chitosan · Nanocomposite · Monolith · Cr(VI) removal

✉ Liang Li
msell08@163.com

✉ Xianghua Yu
yuxianghua05@163.com

[1] Key Laboratory for Green Chemical Process of Ministry of Education, Hubei Key Laboratory of Plasma Chemistry and Advanced Materials, School of Materials Science and Engineering, Wuhan Institute of Technology, Wuhan 430073, People's Republic of China

[2] School of Physical Science and Technology, Yili Normal University, Yining 835000, China

Introduction

In decade years, conducting polymers have been widely applied as the potential materials in the fields of electrocatalysis, chemical or biological sensors, supercapacitors, artificial muscles, electronic devices and protective coatings [1–5]. Of the major conducting polymers, polypyrrole (PPy) has attracted tremendous interest due to its favorable biocompatibility, good electrical conductivity, moderate band gap and reversible electrochemical properties [6–9]. Various methods for the preparation of PPy with different micro/nanostructures have been developed, including template synthesis, interfacial synthesis, and electrochemical polymerization [10–12]. Although the research progress of PPy in morphology and structure control, functionalization and practical applications is significant, most of the as-prepared PPy so far have the macroscopic appearance of insoluble granular powder or intractable thin film. Thus, it has seriously restricted its efficient application because of processing difficulty. Hence, more attention has been paid to the improvement of synthesis method for the fabrication of PPy or its nanocomposites with enhanced processibility in order to overcome the above disadvantage and meet more strict requirements in future applications.

Recently, the pioneering researches about the preparation of PPy and its nanocomposites with three-dimensional network, such as hydrogel, aerogel, sponge, have been reported [13–20]. The unique three-dimensional products based on PPy and its nanocomposites endow them synergistic performances of conducting polymer and hierarchical interconnected open micro/nanostructure. For instance, three-dimensional porous nanostructured PPy hydrogel with good mechanical property and high performance supercapacitor has prepared via interfacial polymerization [21]. The elastic and conducting PPy hydrogel has been synthesized

in the following conditions of mixed solvent, deficient oxidant and monthly growth [22]. PPy nanofiber or nanotube hydrogel with controlled morphology has been synthesized by oxidative polymerization with the aid of liquid crystal molecules or dye molecules as the template and dopant through self-assembly of the interconnected nanoblocks [23–25]. PPy/graphene hydrogel nanocomposites have been fabricated by hydrothermal reduction of graphene oxide and polymerization of pyrrole, resulting in the three-dimensional mesoporous microstructure with PPy wrapped on the surface of graphene hydrogel [26]. We also studied the effect of feed order on the self-assembly of the nanocomposite hydrogel of PPy and chitosan (CS) [27].

It is well-known that CS is a natural polysaccharide derived from chitin and can be used as one of the promising low-cost adsorbents with high adsorption capacity of heavy transition metal ions and dyes [28–30]. Cr(VI) ions are one kind of the most toxic and carcinogenic to human health and environmental quality [31]. It has been reported that PPy and CS could be able to remove Cr(VI) ions from waste water [32–36]. It is desirable to incorporate natural polymer, such as CS, into PPy since such a characteristic is highly beneficial for efficient adsorption. It is expected that the combination of PPy and CS could improve the properties of both PPy and CS. However, most of these PPy/CS nanocomposites are in the form of powder. Therefore, great efforts have been devoted to the exploring and utilizing the three-dimensional network in order to realize the fast and efficient separation of the adsorbents from the effluent after adsorption.

In general, the formation of three-dimensional network based on conducting polymer and natural polymer is realized either by the polymerization of monomer inside the preformed natural polymer hydrogel or by the chemical grafting of conducting polymer on the natural polymer followed with the elaboration of composite hydrogels through crosslinking [37, 38]. For the former, conducting polymer may migrate from the hydrogel network because it is entrapped in the crosslinked matrix of natural polymer hydrogel. Moreover, it is difficult to guarantee the uniform distribution of conducting polymer in the hydrogel. For the latter, the procedure is time-consuming and inconvenient. Although the previous works about the synthesis of three-dimensional PPy-based materials are exciting, the self-standing three-dimensional PPy/CS nanocomposite aerogel monoliths are rarely reported. In the present work, PPy/CS nanocomposite aerogel monoliths are prepared through the simultaneous polymerization and crosslinking technique coupled with freeze drying. The static polymerization of pyrrole monomer using MO as the dopant and APS as the oxidant and the cross-linking of CS by glutaraldehyde take place simultaneously, resulting in the self-assembly of polypyrrole/chitosan nanocomposite aerogel monolith. The one-dimensional PPy nanoblocks and crosslinked CS are responsible for the construction and stabilization of the three-dimensional network, respectively. Herein, we also demonstrate the ability of the as-synthesized PPy/CS nanocomposite aerogel monoliths to remove Cr(VI) ions in aqueous solution. There are two advantages for PPy/CS nanocomposite aerogel monolith as an adsorbent for Cr(VI) removal. Firstly, the hierarchical structures composed of one-dimensional PPy nanoblocks and crosslinked CS with larger specific surface area are beneficial for the efficient adsorption of Cr(VI) ions, thus enhancing the adsorption efficiency of PPy/CS nanocomposite. Secondly, the aerogel monolith could be easily separated from effluent due to its stable monolithic shape.

Experimental

Materials

Ammonium peroxysulfate (APS), methyl orange (MO), and other reagents were used as received. Pyrrole was distilled and kept in the refrigerator before use. Chitosan with viscosity-average molecular weight of 186,000 g/mol and deacetylation degree of 86% was supplied by Zhejiang Golden-Shell Co., Ltd., China.

Fabrication of the Aerogel Monoliths

CS was dissolved in 2% aqueous acetic acid solution to get the concentration of 2 wt%. Then, 1 mmol of APS and 20 mL of 5 mmol L^{-1} MO solution were added in the CS solution with stirring. Some red flocculent could be observed immediately in the beaker. Then the mixture solution was continued to ultra-sonicate for about 3 min. Subsequently, 1 mmol of pyrrole monomer and glutaraldehyde solution were introduced to the above mixture with stirring for several minutes. After that, the reaction was carried out without stirring for 24 h at room temperature to obtain a black hydrogel precursor. The hydrogel precursor was repeatedly rinsed with deionized water and then freeze-dried. The as-prepared aerogel monolith was designated as PPy-c-CS. The schematic procedure is presented in Fig. 1. For comparison, the nanocomposite of PPy and CS was also prepared without the addition of glutaraldehyde. It was designated as PPy–CS.

Characterizations

Fourier transform infrared (FTIR) spectra were performed using Nicolet Impact-420 spectrometer. The morphology of the aerogel was analyzed by a JSM-5510LV scanning electron microscopy (SEM). Nitrogen sorption isotherms (Micromeritics ASAP 2010M instrument) were carried out to study the specific surface area using the Brunauer–Emmett–Teller (BET) measurement. X-ray

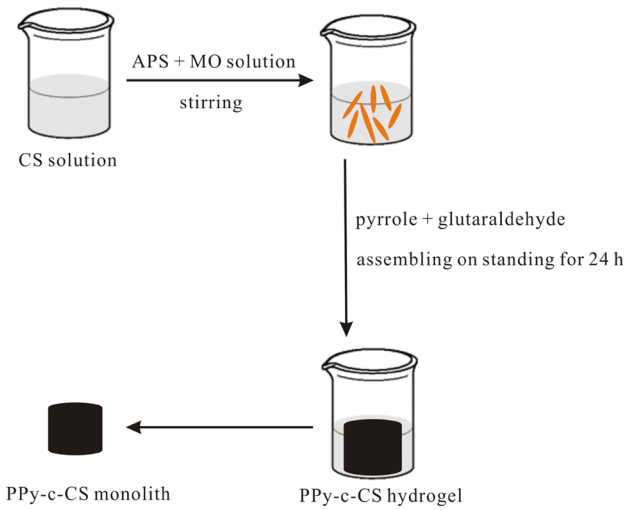

Fig. 1 Scheme showing the preparation process of PPy-c-CS nanocomposite aerogel monolith

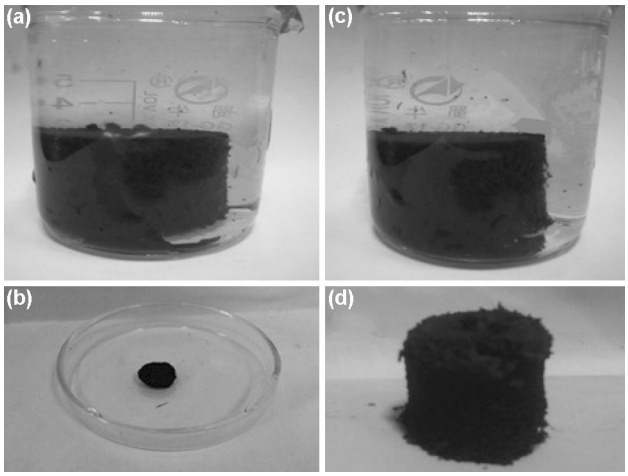

Fig. 2 Photographs of **a, b** PPy–CS and **c, d** PPy-c-CS before and after freeze-drying

photoelectron spectroscopy (XPS) was conducted under a base pressure of 1×10^{-9} Torr using an AXIS Ultra spectrometer.

For the experiments of Cr(VI) removal, the aqueous solution containing Cr(VI) was obtained by dissolving $K_2Cr_2O_7$ at pH 2.0 in water. The as-prepared aerogel monolith was added into 60 mL of Cr(VI) solution with the desired concentration and then stirred. After a certain time, the concentration of Cr(VI) in the solution was analyzed by a ultraviolet spectrophotometer (SHIMADZU UV-2501) according to the standard solutions of Cr(VI) solution. The adsorption capacity of Cr(VI) was calculated using the following formula,

$$q_t = (C_0 - C_t)V/m$$

where q_t (mg/g) was the adsorption capacity at a certain time, C_0 and C_t (mg/L) were the initial concentration of Cr(VI) and the concentration of Cr(VI) at a certain time, respectively, V (L) was the solution volume and m (g) was the mass of adsorbent.

Results and Discussion

In our study, the polymerization of pyrrole using MO as the dopant and APS as the oxidant took place, accompanied with the crosslinking of CS by glutaraldehyde. At the same time, the evolution of hydrogel precursor occurred on standing for 24 h. After freeze-drying, the dried aerogel basically kept the shape and volume of the hydrogel and the corresponding PPy-c-CS aerogel monolith was obtained, as shown in Fig. 2. For comparison, PPy–CS was also prepared with the same procedure just in the absence of glutaraldehyde. It was worth noting that the experimental phenomena before freeze-drying were similar regardless of the addition of glutaraldehyde. The black cylinder whole appeared. However, PPy–CS had totally different macroscopic appearance after freeze-drying and an extraordinary shrinkage of the original hydrogel was observed (Fig. 2). It indicated that it was not enough stable for PPy–CS prepared in the absence of glutaraldehyde to remain the original state during freeze-drying and the sublimation of water from the hydrogel destroyed the initial three-dimensional network. On the other hand, PPy/CS nanocomposites were prepared in the absence of MO or with stirring. The aerogel monolith could not also be obtained in the above two cases. Thus, it was noted that MO, glutaraldehyde and the static condition were required for the fabrication of PPy-c-CS nanocomposite aerogel monolith.

The chemical structure and morphology of PPy-c-CS aerogel monolith were investigated by FTIR and SEM as show in Fig. 3. The characteristic absorbance bands of PPy and CS could be observed. For example, the peak located at 1636 cm^{-1} was ascribed to the C=O stretching vibration of –NHCO– in CS. The peaks located around 1551 and 1482 cm^{-1} corresponded to C=C and C–N asymmetric and symmetric stretching vibration of pyrrole ring, respectively. The peak at 780 cm^{-1} was attributed to C–H ring-wagging vibration of pyrrole [39]. As shown in SEM image, the as-prepared aerogel monolith was composed of one-dimensional nanoblocks together with several nanoparticles. The one-dimensional nanoblocks had the diameter of about 100 nm and the length of several micrometers. The one-dimensional nanostructure of PPy could be prepared using the soft template of MO [40]. Obviously, the simultaneous occurrence of the static polymerization of PPy and the crosslinking of CS influence the morphology of PPy. There were a large number of interconnected one-dimensional nanoblocks. Moreover, several nanoparticles were

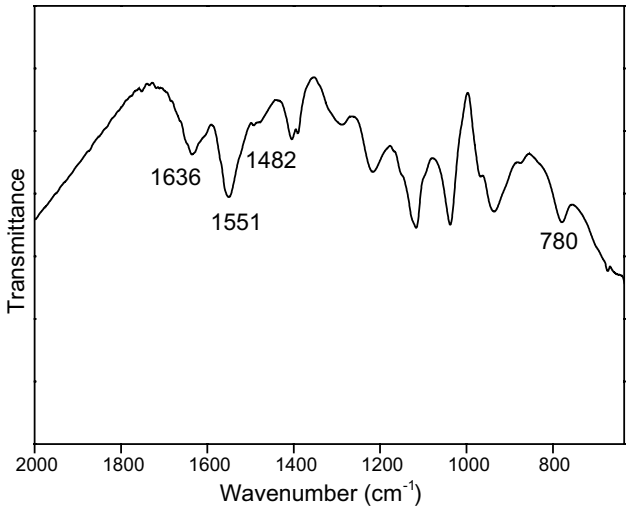

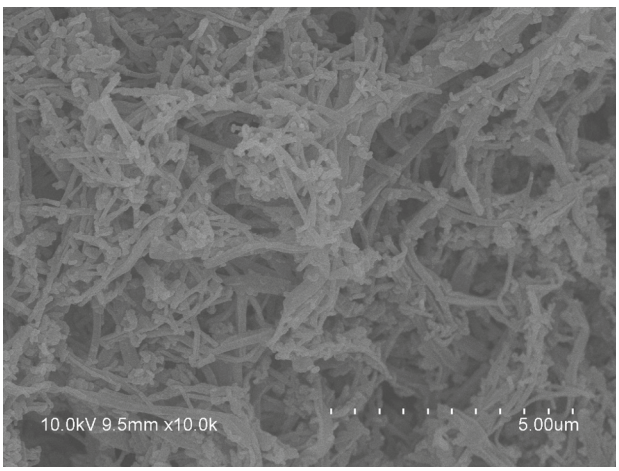

Fig. 3 FTIR spectrum and SEM image of PPy-c-CS

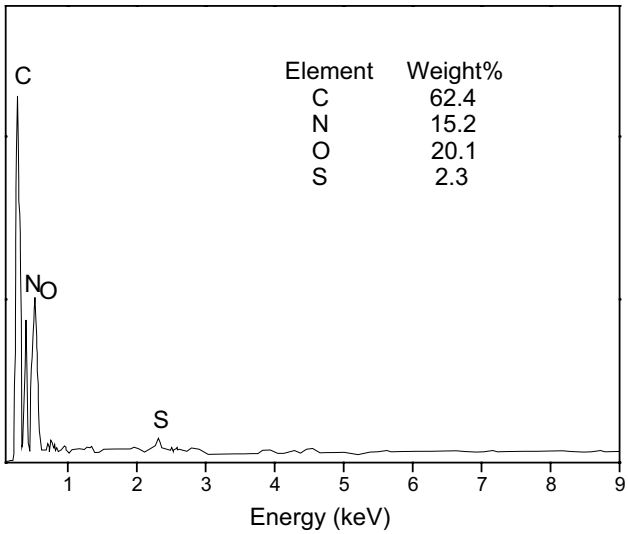

Fig. 4 Energy-dispersive X-ray (EDX) spectrum of PPy-c-CS

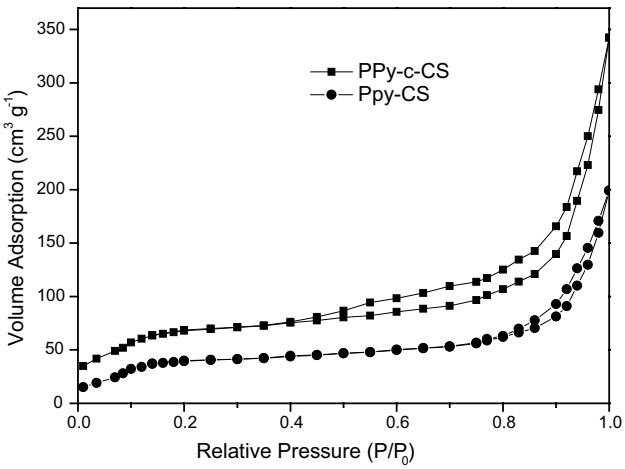

Fig. 5 Nitrogen adsorption/desorption isotherms of PPy–CS and PPy-c-CS

distributed more uniformly among the one-dimensional nanoblocks, compared with that of the nanocomposites of PPy and CS prepared without the addition of glutaraldehyde in our previous study [27]. The bundles and junctions resulting from one-dimensional nanoblocks and several nanoparticles may be more beneficial to the stability of the aerogel monoliths. The N element content in PPy-c-CS nanocomposite was measured by the EDX analysis (Fig. 4). The weight fractions of N element in the nanocomposite was 15.2%. Base on the N content in pure PPy or CS, it was calculated that PPy content and CS content in the nanocomposite was about 59.7 and 40.3%, respectively.

The microstructures of PPy–CS and PPy-c-CS were further investigated by nitrogen adsorption/desorption experiments as shown in Fig. 5. The nitrogen adsorption/desorption isotherms of both PPy–CS and PPy-c-CS exhibited mesoporous characteristics. Based on the nitrogen adsorption experiment, the BET surface area of PPy-c-CS (235 $m^2\ g^{-1}$) was much larger than that of PPy–CS (96 $m^2\ g^{-1}$) (Table 1). The porosity of PPy-c-CS was about 98.9%. It suggested that the PPy-c-CS nanocomposite aerogel monolith obtained in our work had well-developed three-dimensional porous nanostructures and interconnected networks, which could be favorable for the fast ionic transport.

Table 1 BET surface area and kinetics parameters for Cr(VI) adsorption on PPy-c-CS and PPy–CS

Sample	BET ($m^2\ g^{-1}$)	q_e (mg g^{-1})	k_2 (g $mg^{-1}\ min^{-1}$)	r^2
PPy-c-CS	235	350	4.63×10^{-5}	0.998
PPy–CS	96	140	1.35×10^{-4}	0.997

The rich functional groups of the conducting PPy endowed it with the ability to absorb Cr(VI) easily. Meanwhile, CS could bind metal cations through the interaction between the void orbital of the metal and the free electron pairs of the nitrogen. Therefore, the larger specific surface area and the stable macroscopic shape of the obtained PPy-c-CS aerogel monolith afforded its potential as an efficient absorbent for the removal of Cr(VI) ions. Figure 6a showed the effects of adsorption time on adsorption capacity of PPy-c-CS and PPy–CS. The difference of the adsorption behavior between PPy-c-CS and PPy–CS was obvious. The equilibrium adsorption capacity of Cr(VI) ions for PPy-c-CS was much higher than that of PPy–CS. Pseudo-second-order kinetic model was used to evaluate the adsorption performance of PPy-c-CS and PPy–CS. The adsorption kinetics was simulated by the following pseudo-second-order kinetic equation [41]:

$$\frac{t}{q_t} = \frac{1}{k_2 q_e^2} + \frac{t}{q_e}$$

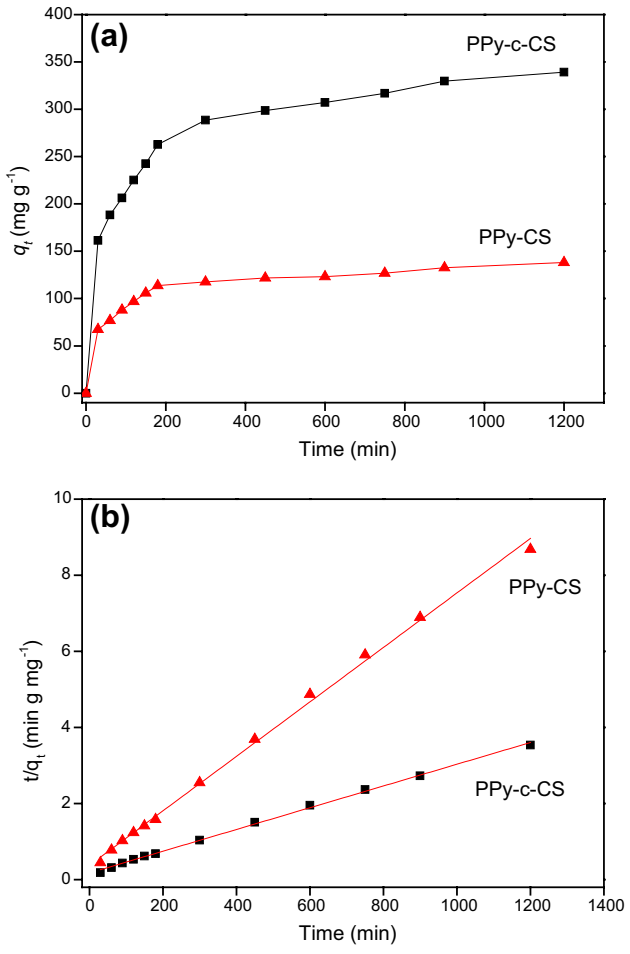

Fig. 6 **a** Effects of adsorption time on adsorption capacity of PPy-c-CS and PPy–CS (initial concentration 100 mg L^{-1}). **b** Pseudo-second-order kinetic model of PPy-c-CS and PPy–CS

where q_e was the equilibrium Cr(VI) adsorption capacity, q_t was Cr(VI) adsorption capacity at a certain time and k_2 was the pseudo-second-order rate constant, respectively. The adsorption data was shown in Fig. 6b and Table 1. The equilibrium Cr(VI) adsorption capacity (q_e) of PPy-c-CS and PPy-CS was calculated to be 350 and 140 mg g^{-1}, while both of the behaviors were linear with correlation coefficient $r^2 = 0.998$ and 0.997 for PPy-c-CS and PPy-CS, respectively. It indicated that PPy-c-CS with stable monolith had the better performance of Cr(VI) removal than the shrunk PPy-CS.

Moreover, the Langmuir model was used to describe the adsorption thermodynamics of PPy-c-CS using the following equation [41]:

$$\frac{C_e}{q_e} = \frac{1}{k_L q_m} + \frac{C_e}{q_m}$$

where C_e was the equilibrium concentration of Cr(VI), q_m was the maximum adsorption capacity per weight of adsorbent, and k_L was the Langmuir adsorption constant, respectively. Cr(VI) adsorption isotherm curves of PPy-c-CS and the fit of equilibrium data to Langmuir isotherm model was shown in Fig. 7 and Table 2. Based on the fitting results, the adsorption data of Cr(VI) ions were simulated well with the Langmuir model. The maximal Cr(VI) adsorption capacity (q_m) of PPy-c-CS was about 401 mg g^{-1}, which was close to the experimental value shown in Fig. 5. A comparison of the Langmuir maximum adsorption capacity between PPy-c-CS and other PPy-based adsorbents reported in literatures had been conducted. The adsorption capacity of PPy-c-CS nanocomposite was higher than that of Fe_3O_4/PPy microsphere (209 mg g^{-1}) [42], that of PPy-polyaniline nanofibers (227 mg g^{-1}) [35], that of porous PPy nanoclusters (180 mg g^{-1}) [43], that of PPy/CS nanocomposite (79 mg g^{-1}) [36]. Although Cr(VI) adsorption capacity was lower than PPy@GO nanocomposite (497 mg g^{-1}) [44], our PPy-c-CS nanocomposite could be conveniently separated from effluent due to its stable monolithic shape.

XPS spectrum of PPy-c-CS after Cr(VI) adsorption was given in Fig. 8 in order to investigate the mechanism of Cr (VI) adsorption by PPy-c-CS. Two main energy bands at about 577.2 and 587.3 eV appeared, which could be ascribed to the binding energies of Cr $2p_{3/2}$ and Cr $2p_{1/2}$. It suggested that there existed Cr(III) and Cr(VI) ions in PPy-c-CS after the adsorption. The existence of Cr(III) in PPy-c-CS proved that some portion of adsorbed Cr(VI) ions was reduced to Cr(III) by PPy component during the adsorption process [45]. The regeneration ability and stability of the adsorbent was crucial for its practical application. In our work, the adsorbent was first desorbed by dipping in 0.5 mol L^{-1} NaOH solution and then recycled in 1 mol L^{-1} HCl solution [45]. Figure 9 showed the adsorption cycles of PPy-c-CS for removal of Cr(VI).

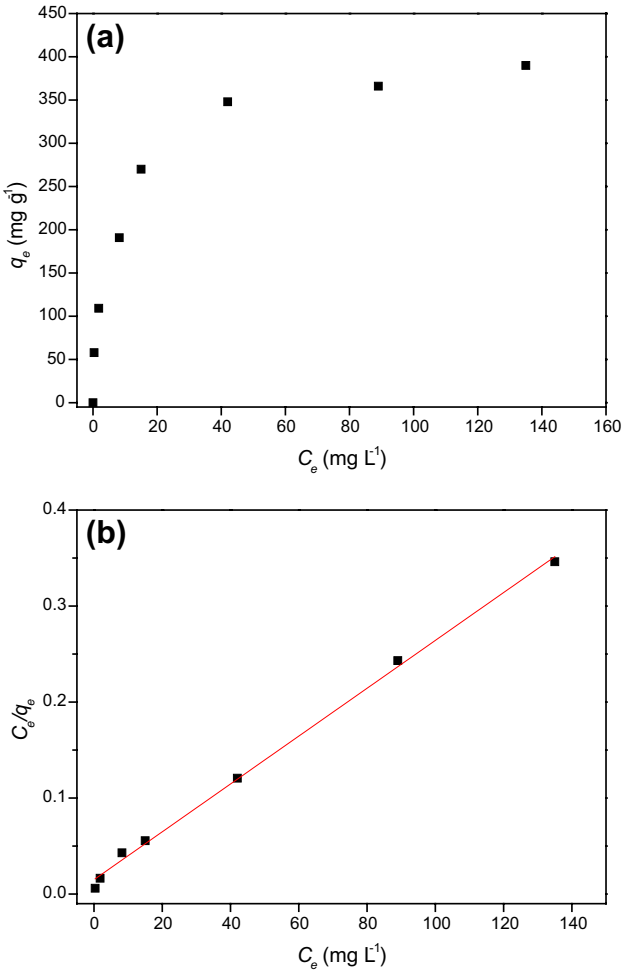

Fig. 7 **a** Cr(VI) adsorption isotherm curves of PPy-c-CS. **b** Fit of equilibrium data to Langmuir isotherm model

Table 2 Langmuir constants for Cr(VI) adsorption on PPy-c-CS

Metal ion	q_m (mg g^{-1})	k_L (L mg^{-1})	r^2
Cr(VI)	401	0.166	0.997

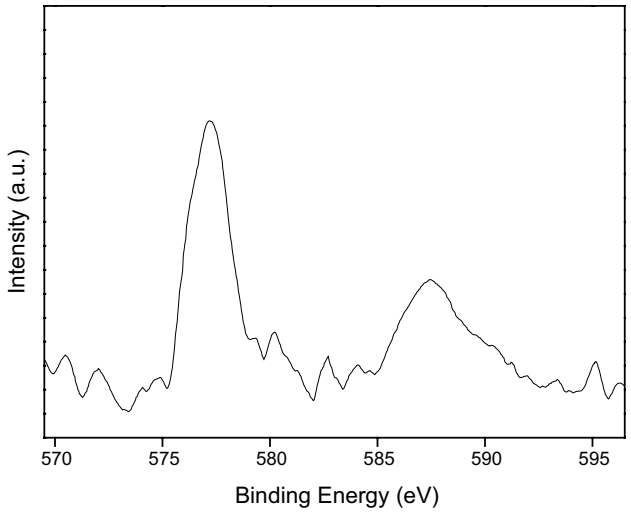

Fig. 8 XPS spectrum of PPy-c-CS after Cr(VI) adsorption

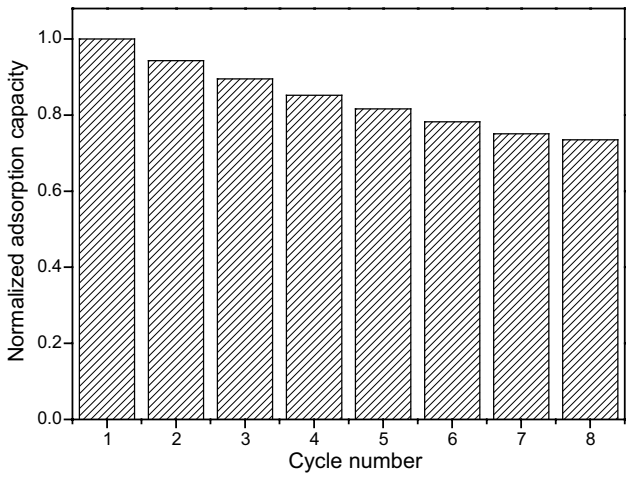

Fig. 9 Adsorption cycles of PPy-c-CS for removal of Cr(VI)

After eight cycles of the adsorption–desorption process, about 73.5% of the Cr(VI) removal ability remained, which indicated that PPy-c-CS was suitable to be used as a recyclable adsorbent for Cr(VI) ions. Furthermore, after eight adsorption–desorption cycles, PPy-c-CS could still be easily separated from the solution due to its stable monolithic structure.

Conclusions

An effective static route for the fabrication of PPy-c-CS nanocomposite aerogel monoliths with three-dimensional framework has been presented. The self-standing PPy-c-CS nanocomposite aerogel monoliths are prepared by self-assembly of PPy-c-CS nanocomposite hydrogel precursors and subsequent freeze-drying. The formation and the properties of these monoliths depend strongly on the reaction condition, such as the dye dopant, stirring and crosslinking agent. Due to the synergic effect between one-dimensional polypyrrole blocks and crosslinked chitosan, PPy-c-CS nanocomposite aerogel monolith is a suitable adsorbent for the efficient removal of Cr(VI). The successful synthesis of self-standing aerogel monoliths based on conducting polymer and natural polymer may be extended to construct other nanocomposite aerogel analogues for potential applications in future.

Acknowledgements The work was supported by Outstanding Youth Scientific Innovation Team of Colleges and Universities in Hubei Province (T201406), National Natural Science Foundation of China (51403167), Graduate Innovative Fund of Wuhan Institute of Technology (CX2016001), and Training Programs of Innovation and Entrepreneurship for Undergraduates (201610490019).

References

1. Bavio MA, Acosta GG, Kessler T (2014) J Power Sources 245:475
2. Pernites RB, Ponnapati RR, Advincula RC (2011) Adv Mater 23:3207
3. Yatsyshyn M, Saldan I, Milanese C, Makogon V, Zeffiro A, Bellani V, Lorenzo R, Cofrancesco P, Girella A, Dondi D, Reshetnyak O, Korniy S (2016) J Polym Environ 24:196
4. Liu F, Yuan Y, Li L, Shang S, Yu X, Zhang Q, Jiang S, Wu Y (2015) Comp Part B Eng 69:232
5. Kwon OS, Park E, Kweon OY, Park SJ, Jang J (2010) Talanta 82:1338
6. Dubal DP, Lee SH, Kim JG, Kim WB, Lokhande CD (2012) J Mater Chem 22:3044
7. Ansari R, Delavar AF (2010) J Polym Environ 18:202
8. Liu SL, He K, Wu X, Luo XG, Li B (2015) RSC Adv 5:87266
9. Samanta D, Meisera JL, Zare RN (2015) Nanoscale 7:9497
10. Liu Z, Zhang X, Poyraz S, Surwade SP, Manohar SK (2010) J Am Chem Soc 132:13158
11. Qi G, Huang L, Wang H (2012) Chem Commun 48:8246
12. West R, Zeng X (2008) Langmuir 24:11076
13. Temmer R, Kiefer R, Aabloo A, Tamm T (2013) J Mater Chem A 1:15216
14. Ying S, Zheng W, Li B, She X, Huang H, Li L, Huang Z, Huang Y, Liu Z, Yu X (2016) Synth Met 218:50
15. Brahim S, Narinesingh D, Guiseppi-Elie A (2002) Biosens Bioelectron 17:973
16. Zhou S, Wang M, Chen X, Xu F (2015) ACS Sustain Chem Eng 3:3346
17. Tuo X, Li B, Chen C, Huang Z, Huang H, Li L, Yu X, (2016) Synth Met 213:73
18. Jiang T, Sui Z, Yang Q, Zhang X, Han B (2015) Soft Matter 11:3215
19. Ji J, Yu X, Cheng P, Zhang Q, Du F, Li L, Shang S (2015) J Macromol Sci Part B Phys 54:1122
20. Mekonnen BT, Ragothaman M, Kalirajan C, Palanisamy T (2016) RSC Adv 6:63071
21. Shi Y, Pan L, Liu B, Wang Y, Cui Y, Bao Z, Yu G (2014) J Mater Chem A 2:6086
22. Lu Y, He W, Cao T, Guo H, Zhang Y, Li Q, Shao Z, Cui Y, Zhang X (2014) Sci Rep 4:5792
23. Wang Y, Shi Y, Pan L, Ding Y, Zhao Y, Li Y, Shi Y, Yu G (2015) Nano Lett 15:7736
24. Wei D, Lin X, Li L, Shang S, Yuen MC, Yan G, Yu X (2013) Soft Matter 9:2832
25. Dai T, Lu Y (2007) J Mater Chem 17:4797
26. Zhang F, Xiao F, Dong ZH, Shi W (2013) Electrochim Acta 114:125
27. Huang H, Wu J, Lin X, Li L, Shang S, Yuen MC, Yan G (2013) Carbohydr Polym 95:72
28. Chauhan D, Jaiswal M, Sankararamakrishnan N (2012) Carbohydr Polym 88:670
29. Afzal S, Samsudin EM, Julkapli NM, Abd Hamid SB (2016) Environ Sci Poll Res 23:23158
30. Yun YH, Yun JW, Yoon SD, Byun HS (2016) Macromol Res 24:51
31. Yusof AM, Malek N.A.N.N. (2009) J Hazard Mater 162:1019
32. Wei C, German S, Basak S, Rajeshwar K (1993) J Electrochem Soc 140:60
33. Ngah W, Teong LC, Hanafiah M (2011) Carbohydr Polym 83:1446
34. Lei Y, Qian X, Shen J, An X (2012) Ind Eng Chem Res 51:10408
35. Bhaumik M, Maity A, Srinivasu VV, Onyango MS (2012) Chem Eng J 181–182:323
36. Karthik R, Meenakshi S (2015) Desalin Water Treat 56:1587
37. Xiao Y, He L, Che J (2012) J Mater Chem 22:8076
38. Marcasuzaa P, Reynaud S, Ehrenfeld F, Khoukh A, Desbrieres J (2010) Biomacromolecules 11:1684
39. Yang X, Li L, Yan F (2010) Sens Actuators B Chem 145:495
40. Yang X, Li L (2010) Synth Met 160:1365
41. Kampalanonwat P, Supaphol P (2010) ACS Appl Mater Interfaces 2:3619
42. Wang YQ, Zou BF, Gao T, Wu XP, Lou SY, Zhou SM (2012) J Mater Chem 22:9034
43. Yao TJ, Cui TY, Wu J, Chen QZ, Lu SW, Sun KN (2011) Polym Chem 2:2893
44. Li SK, Lu XF, Xue YP, Lei JY, Zheng T, Wang C (2012) PLoS ONE 7:e43328
45. Bhaumik M, Maity A, Srinivasu VV, Onyango MS (2011) J Hazard Mater 190:381